Integrated full-length transcriptome and metabolome analysis reveals the defense response of melon to gummy stem blight

Qiusheng Kong[1], Haiyan Wang[1], Xiaoying Wei[1], Changjuan Mo[1], Minghua Wei[1], Yaqiong Li[1], Yuxin Fan[1], Xiaojing Gu[1], Xuejun Zhang[2], and Yongbing Zhang[2]

[1]Huazhong Agriculture University College of Horticulture and Forestry Sciences
[2]Xinjiang Academy of Agricultural Sciences

March 11, 2024

Abstract

Gummy stem blight (GSB), a severe and widespread disease causing great losses to cucurbit production, is a major threat to melon production. However, the melon-GSB interaction remains largely unknown, which significantly impedes the genetic improvement of melon for GSB resistance. Here, full-length transcriptome and widely targeted metabolome were used to reveal the early defense responses of resistant (PI511890) and susceptible (Payzawat) melon to GSB. Differentially expressed genes were specifically enriched in the secondary metabolite biosynthesis and MAPK signaling pathway in PI511890, while in carbohydrate metabolism and amino acid metabolism in Payzawat. More than 1000 novel genes were identified in PI511890, which were enriched in the MAPK signaling pathway. There were 11,793 alternative splicing events identified and involved the defense response to GSB. A total of 910 metabolites were identified, with flavonoids as the dominant metabolites. Integrated full-length transcriptome and metabolome analysis showed that eriodictyol and oxalic acid may be used as marker metabolites for GSB resistance in melon. Moreover, post-transcription regulation was widely involved in the defense response of melon to GSB. These results improve our understanding of the interaction between melon and GSB and may facilitate the genetic improvement of GSB resistance of melon.

Integrated full-length transcriptome andmetabolome analysis reveals the defense response of melonto gummy stem blight

Haiyan Wang[1], Xiaoying Wei[1], Changjuan Mo[1], Minghua Wei[1], Yaqiong Li[1], Yuxin Fan[1], Xiaojing Gu[1], Xuejun Zhang[2], Yongbing Zhang[2*], Qiusheng Kong[*]

Affiliation

[1] National Key Laboratory for Germplasm Innovation & Utilization of Horticultural Crops; College of Horticulture and Forestry Sciences, Huazhong Agricultural University, Wuhan 430070, China

[2] Hami-melon Research Center, Xinjiang Academy of Agricultural Sciences, Urumqi 830091, China

*Corresponding authors:

Yongbing Zhang: hamimelon@xaas.ac.cn

Qiusheng Kong: qskong@mail.hzau.edu.cn ORCID: 0000-0003-0939-4424

Abstract

Gummy stem blight (GSB), a severe and widespread disease causing great losses to cucurbit production, is a major threat to melon production. However, the melon-GSB interaction remains largely unknown, which significantly impedes the genetic improvement of melon for GSB resistance. Here, full-length transcriptome

and widely targeted metabolome were used to reveal the early defense responses of resistant (PI511890) and susceptible (Payzawat) melon to GSB. Differentially expressed genes were specifically enriched in the secondary metabolite biosynthesis and MAPK signaling pathway in PI511890, while in carbohydrate metabolism and amino acid metabolism in Payzawat. More than 1000 novel genes were identified in PI511890, which were enriched in the MAPK signaling pathway. There were 11,793 alternative splicing events identified and involved the defense response to GSB. A total of 910 metabolites were identified, with flavonoids as the dominant metabolites. Integrated full-length transcriptome and metabolome analysis showed that eriodictyol and oxalic acid may be used as marker metabolites for GSB resistance in melon. Moreover, post-transcription regulation was widely involved in the defense response of melon to GSB. These results improve our understanding of the interaction between melon and GSB and may facilitate the genetic improvement of GSB resistance of melon.

Key words: Melon; Gummy stem blight; Full-length transcriptome; Metabolome

Introduction

Melon (*Cucumis melo* L.), an important horticultural crop with great economic significance, is widely grown for fresh consumption. According to the statistics of Food and Agriculture Organization, the global melon production reached 28.6 million tons in 2021 (FAOSTAT, www.fao.org/faostat). China is the leading producing country of melon, accounting for approximately half of the total production (14.1 million tons), followed by Turkey, India, and Kazakhstan, whose annual production was 1.4–1.6 million tons in 2021. However, the yield and quality of melon are faced with serious threats of diseases caused by pathogen attack.

Gummy stem blight (GSB) caused by *Stagonosporopsis cucurbitacearum* (syn. *Didymella bryoniae*) is a prevalent and devastating fungal disease of melon throughout the world (Li et al., 2017; Stewart et al., 2015). It has been reported that GSB pathogens can attack 37 species of the Cucurbitaceae family (Rennberger & Keinath, 2018). Under favorable environmental conditions, the pathogen can infect all aboveground parts of susceptible plants throughout the whole growth period, causing the formation of necrotic spots and serious reduction of yield and quality. The incidence of GSB can reach up to 80% for melon cultivated in greenhouse, and the yield loss can reach 100% once infected (Rennberger & Keinath, 2018; Virtuoso et al., 2022). Currently, chemical control, particularly fungicides, is the most widely used method to control GSB. However, excessive application of fungicides inevitably causes negative impacts on the environment and food safety. In addition, the effect is declining due to increasing resistance of certain pathogenic isolates to chemicals (Keinath & Zitter, 1998; Hassan et al., 2018).

Breeding of resistant cultivars is the most efficient approach for disease control. In recent years, some research efforts have been devoted to screening GSB-resistant melon germplasm (Wolukau et al., 2007; Zhang et al., 1997). A review has summarized the currently identified melon GSB-resistant resources (Luo et al., 2022). Another study investigated the inheritance of GSB-resistant traits, resulting in the identification of five independent monogenic resistance loci from PI accessions of PI140471, PI157082, PI511890, PI482398, and PI482399, which were designated as *Gsb-1* , *Gsb-2* , *Gsb-3* ,*Gsb-4* , and *gsb-5* , respectively (Frantz & Jahn, 2004). Only a limited number of molecular markers associated with GSB resistance have been developed for maker-assisted selection of melon (Hassan, Rahim et al., 2018; Hassan, Robin et al., 2018; Wolukau et al., 2009). By using an ultra-dense genetic map, a previous study mapped GSB resistance QTLs from an inbred line of *Cucumis melo* spp.*conomon* into a 108-kb interval on chromosome 4 and proposed a candidate gene (Hu et al., 2018). Recently, *Gsb-7(t)* conferring GSB resistance was mapped on chromosome 7 and *MELO3C010403-T2* was proposed as the candidate gene (Ma et al., 2023). However, functions of these candidate genes have not been validated yet (Seblani et al., 2023).

Clarifying the defense response of host to pathogen infection is important for understanding the disease resistance mechanism. High-throughput omics technologies have become powerful tools for studying plant defense response to biotic stresses, among which transcriptome is widely employed to identify the genes, signal transduction pathways, and regulatory networks involved in plant-pathogen interaction. For example, a transcriptomic analysis in a recent study demonstrated that an apyrase-like gene plays an important

role in the defense response of pumpkin to GSB (Zhao et al., 2022). Alternative splicing (AS), which is usually identified by full-length transcriptome, is an important post-transcriptional regulatory mechanism that increases the diversity of transcripts and proteins (Ule & Blencowe, 2019). Several studies have shown that many genes undergo AS in response to biotic stresses in plants (Zhang et al., 2019). Functional analysis of alternative transcripts has become a powerful tool to develop new strategies for improvement of plant tolerance to environmental stress (Kufel et al., 2022). Metabolome can act as a bridge between genotypes and phenotypes, and is also a powerful tool for decoding plant-pathogen interaction (Serag et al., 2023). Disease infection can cause great perturbation on plant metabolism. The widely targeted metabolome allows comprehensive metabolic profiling of plants during pathogen attack. It is known that plant secondary metabolites, including phenolic compounds, alkaloids, glycosides, and terpenoids, play pivotal roles in plant-pathogen interaction (Anjali et al., 2023). However, gene expression profiles, AS landscape, and metabolites involved in the defense response of melon to GSB remain largely unknown.

In this study, we selected two melon accessions with contrasting resistance to GSB, and determined their defense responses to GSB based on full-length transcriptome and widely targeted metabolome. We also characterized the novel genes, AS events, differentially expressed genes (DEGs), and differentially accumulated metabolites (DAMs) involved in the defense response of melon to GSB. The results are expected to provide a comprehensive understanding on the defense response of melon to GSB at transcriptomic and metabolic levels, as well as valuable information for elucidating the mechanism for the resistance of melon to GSB.

Materials and methods

Plant materials and artificial inoculation

PI511890 (*C. melo* var. *chito*) from Mexico and Payzawat from China (*C. melo* var. *inodorus*) were used as the plant materials in this study. PI511890 is a wild melon accession and exhibits resistance to GSB (Frantz & Jahn, 2004). Payzawat is a widely cultivated landrace and susceptible to GSB. The seeds were firstly sterilized with 1.5% sodium hypochlorite, and then sown in pots containing sterilized peat-perlite substrate (2: 1, v/v). The pots were placed in a greenhouse and seedling management followed the commercial production practices. At the third true leaf stage, uniform and healthy seedlings were selected for subsequent experiments.

Pathogenic fungi were isolated from melon stem with typical GSB symptoms and identified as *Stagonosporopsis cucurbitacearum* . Purified fungi were inoculated on potato dextrose agar (PDA) culture medium, cultured at 25 under darkness for three days, then treated with 12 h photoperiod under ultra-violet light (280–360 nm) for five days, and maintained at darkness for two days to obtain the spores. The spores on the medium were washed off and filtered to obtain the spore suspension. The inoculum suspension was adjusted to 5 $\times$ 10^5spores/mL by adding ddH_2O. For inoculation, the spore solution was sprayed on the seedlings until reaching the point of runoff. After inoculation, the seedlings were covered with a plastic tunnel and the relative humidity was kept over 90% with the temperature varying from 25 to 30. At the same time, spraying of distilled water was performed for the other seedlings to be used as the controls. Completely randomized block experimental design with three biological replicates was adopted for the treatments and controls, with each replicate consisting of 20 seedlings. Leaves were sampled at 0, 12, 24, 36, 48, 60, 72 h after inoculation (hpi) for subsequent analyses. For transcriptome and metabolome analyses, the leaves were immediately frozen in liquid nitrogen and then stored in a refrigerator (–80degC).

Histochemical staining

Trypan Blue staining was performed for the leaves to determine the growth of spores and hyphae according to the previous reports (Bhadauria et al., 2010; van Wees, 2008). Briefly, the leaves were punched to discs with a diameter of 10 mm and soaked in the Trypan Blue staining solution, then immediately heated in 90 water for 10 min. After the solution was allowed to cool down to room temperature, the staining solution was discarded and the leaf discs were decolorized using 2.5 mg/mL chloral hydrate solution, which was replaced after every 24 h until the leaf discs were completely decolorized.

Accumulation of H_2O_2 and O^{2-} in leaves was measured using 3,3'-diaminobenzidine (DAB) and nitro blue tetrazolium chloride (NBT) staining methods, respectively (Daudi & O'Brien, 2012). In brief, the leaves were punched into several discs with a diameter of 10 mm. For each biological replicate, 10 discs were selected and immersed in 1 mg/mL DAB solution under 25 /light for 5 h and 0.5 mg/mL NBT solution under 25 /dark for 5 h, respectively. Then, the leaf discs were decolorized with 95% ethanol under 95 for 20 min and immersed in anhydrous ethanol for store and photo. The staining results were observed under a light optical microscope (OLYMPUS C x 41) with an ocular magnification lens at 40 x (400 um scale). The staining areas were calculated using Image J with the formula of (stained leaf area/leaf disc area) x 100% (Schneider et al., 2012). The larger staining area means higher accumulation of H_2O_2 or O^{2-}. ANOVA was used to test the differences in staining areas among treatments and the least significant difference was used for multiple comparisons of the means. The agricolae package of R was used for statistical analysis.

Full-length transcriptome analysis

Samples at 24 hpi were selected for full-length transcriptome analysis, which included GSB-inoculated samples of PI511890 (TRT) and Payzawat (TST), and controls of PI511890 (TRC) and Payzawat (TSC). Extraction of RNA and construction of sequencing libraries were performed according to the protocols providing by the Oxford Nanopore Technologies (ONT). The libraries were sequenced on a PromethION platform to obtain the full-length transcriptome according to the standard protocol of ONT.

The pipeline for full-length transcriptome analysis is shown in Supplementary Figure 1. The short fragments and low-quality reads (length $<$ 100 bp, Qscore $<$ 7) were filtered out using NanoFilt (v2.8.0; Coster et al., 2018). The clean data were then processed with Pychopper (v2.4.0) to identify and orient full-length sequences. The melon genome of DHL92 (v4.0) was used as the reference (http://cucurbitgenomics.org/v2/organism/23). The full-length sequences were mapped to the reference genome using minimap2 (v2.17-r941; Li, 2018). Samtools (v1.7) was used to extract the uniquely mapped reads with a minimum quality score of 10. After polishing and clustering the full-length sequences, the consensus sequence was obtained using Pinfish pipeline (v0.1.0; Chen et al., 2021). The resulting consensus transcripts were then mapped to the reference genome using minimap2.

Transcript isoforms were identified for the full-length transcriptome. All consensus transcripts were merged and assembled to obtain a non-redundant transcript set using StringTie (Pertea et al., 2015). The assembled transcripts were compared with the reference genome using gffcompare (v0.12.1; Pertea & Pertea, 2020). After filtering transcripts with single exon, transcripts with class codes ("u", "x", "i", "j", "o") and length longer than 200 bp were defined as novel transcripts. The novel transcripts were further classified into isoforms of novel genes ("u", "x", "i") and novel isoforms of known genes ("j", "o").

Ballgown was used to estimate transcript abundance (v2.26.0; Pertea et al., 2016). DEGs were identified using DEseq2 with $|\log_2\text{FoldChange}| > 1$ and adjusted $p < 0.05$ (Liu et al., 2021). Enrichment analyses of Gene Ontology (GO) and Kyoto Encyclopedia of Genes and Genomes (KEGG) for DEGs were performed using clusterProfiler with the cutoff of $p < 0.05$ (Yu et al., 2012).

AS events and fusion genes were identified. SUPPA2 (v2.3) was used to generate seven main types of the local AS events, including retained intron (RI), alternative 5' splice-site (A5), alternative 3' splice-site (A3), skipping exon (SE), alternative first exon (AF), alternative last exon (AL), and mutually exclusive exons (MX) (Trincado et al., 2018). Salmon (v0.13.1) was used to calculate the transcript abundance (TPM), which was then used to calculate the value of percentage spliced-in (PSI) by SUPPA2 (Patro et al., 2017). Furthermore, diffSplice was applied to identify differentially alternative splicing events with the cutoff of $p < 0.05$ (Hu et al., 2013). Candidate fusion genes were identified using the ToFU (fusion_finder.py) in cDNA_Cupcake program (v29.0.0, https://github.com/Magdoll/cDNA_Cupcake).

Widely targeted metabolome analysis

The samples at 24 hpi were further selected for widely targeted metabolome analysis, which included GSB-inoculated samples of PI511890 (MRT) and Payzawat (MST), and controls of PI511890 (MRC) and Payzawat

(MSC). Extraction, detection, identification, and quantification of metabolites were performed according to the reported methods (Chen et al. 2013). Briefly, the freeze-dried sample was crushed using a mixer mill (MM 400, Retsch) with a zirconia bead for 1.5 min at 30 Hz, and approximately 100 mg of powder was extracted with 70% aqueous methanol. The sample extracts were analyzed using an ultra-performance liquid chromatography-electrospray ionization-mass spectrometry (UPLC-ESI-MS/MS) system (UPLC, Shim-pack UFLC SHIMADZU CBM30A system; MS, Applied Biosystems 4500 Q TRAP). The analytical conditions were as follows, UPLC: column, Agilent SB-C18 (1.8 μm, 2.1 mm × 100 mm); column temperature, 40°C; flow rate, 0.35 mL/min; injection volume, 4 μL. LIT and triple quadrupole (QQQ) scans were acquired on a triple quadrupole-linear ion trap mass spectrometer (Q TRAP). Instrument tuning and mass calibration were performed with 10 and 100 μmol/L polypropylene glycol solutions in QQQ and LIT modes, respectively. A specific set of MRM transitions were monitored for each period according to the metabolites eluted within this period.

Based on the detected metabolites, principal component analysis (PCA) was performed to reveal the relationships among the samples using FactoMineR and factoextra packages in R. The orthogonal partial least squares-discriminant analysis (OPLS-DA) was performed to determine the DAMs with $|\log_2\text{FoldChange}| > 1$ and variable importance in project (VIP) [?]1 (Eriksson et al., 2006). Enrichment analysis for DAMs was conducted using the Metabolites Biological Role (MBROLE) (v2.0; López-Ibáñez et al., 2016).

3. Results

3.1 Growth of GSBpathogenic fungi on melon leaves

The growth process of *S. cucurbitacearum* on the leaves of PI511890 and Payzawat was observed at 0, 12, 24, 36, 48, 60, and 72 hpi using trypan blue staining method. The results showed that the growth process of *S. cucurbitacearum* consisted of germination of conidia, formation and elongation of germ tube, production of appresorium, as well as growth and spread of hyphae (Figure 1A). On the leaves of Payzawat (GSB-susceptible), germ tubes and hyphae were observed at 12 hpi, followed by appressoria at 24 hpi. The hyphae were apparently elongated at 60 hpi and even began to invade into epidermis of Payzawat leaves at 72 hpi. However, on the leaves of PI511890 (GSB-resistant), germ tubes and appressoria appeared until 24 hpi and 36 hpi, respectively. Hyphae were observed at 60 hpi, which grew slowly thereafter. These results indicated that the spore germination and hyphal growth of *S. cucurbitacearum* on PI511890 leaves were inhibited compared with those on Payzawat leaves. Moreover, 24 hpi was the key time point to determine the different responses of PI511890 and Payzawat to *S. cucurbitacearum* infection.

3.2 Accumulation of H_2O_2 and O^{2-} in melon leaves after GSB infection

Accumulation of H_2O_2 and O^{2-} in the leaves of PI511890 and Payzawat was determined using DAB and NBT staining methods at 12, 24, 36, and 48 hpi, respectively. The results of DAB staining showed that H_2O_2 accumulation in infected leaves was higher than that in the control for both Payzawat and PI511890, indicating that GSB promotes H_2O_2accumulation (Figure 1B). Compared with the control, significantly higher accumulation of H_2O_2 was observed in Payzawat after 24 hpi (Figure 1D). However, significantly higher accumulation of H_2O_2 was only observed at 24 hpi in infected leaves of PI511890 compared with the control. Moreover, H_2O_2 accumulation in infected leaves of Payzawat was consistently higher than that of PI511890. Similar accumulation patterns of O^{2-} were also observed in the leaves of Payzawat and PI511890, indicating that GSB also induces the accumulation of O^{2-} (Figure 1C). Additionally, O^{2-} accumulation in infected leaves of Payzawat was significantly higher than that of PI511890 at 24 hpi (Figure 1E). The lower accumulation of H_2O_2 and O^{2-} in PI511890 suggested that reactive oxygen homeostasis is possibly involved in the resistance to GSB.

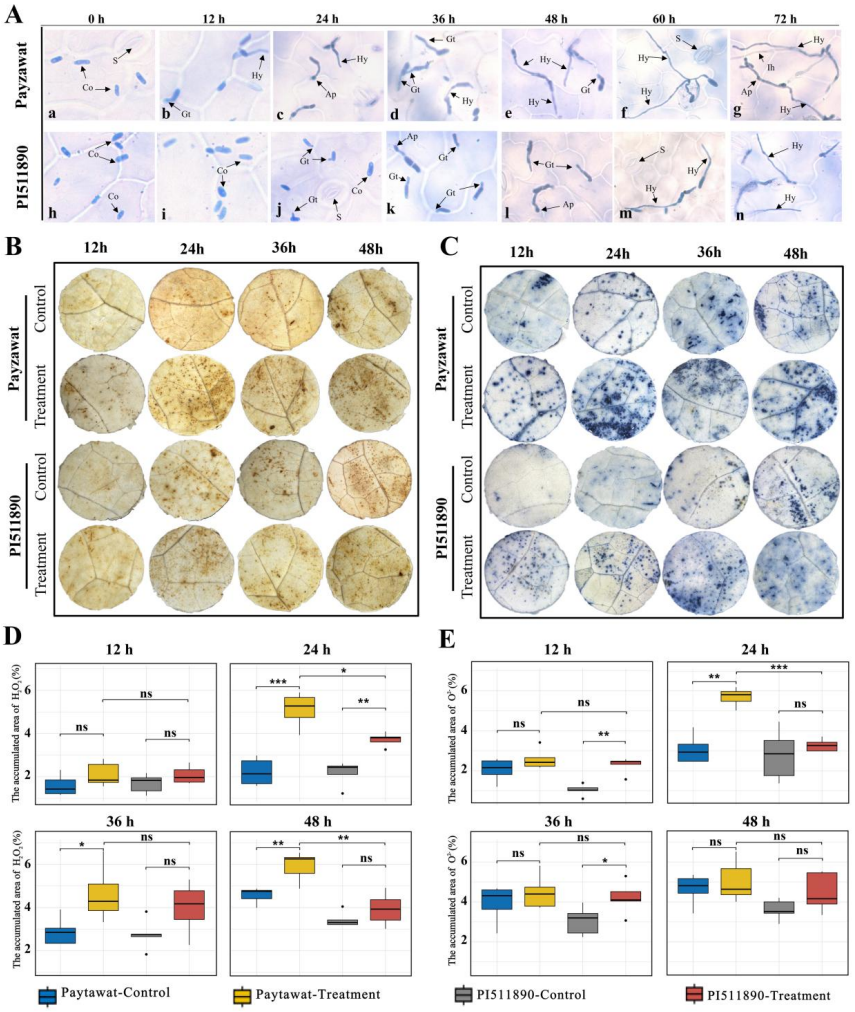

Figure 1 Growth of GSB pathogenic fungi and accumulation of H_2O_2 and O^{2-} in leaves of PI511890 and Payzawat. **A** : Growth of GSB pathogens on the leaves of Payzawat and PI511890 (40 ×). Co, Gt, Ap, Hy, Ih, and S represent conidium, germ tube, appresorium, hyphae, infection hyphae, and stoma, respectively. **B** : Leaves of Payzawat and PI511890 stained by diaminobenzidine at different time points after*S. cucurbitacearum* inoculation. Payzawat-control and PI511890-control are the control groups sprayed with ddH_2O. Payzawat-treatment and PI511890-treatment are the treatment groups sprayed with the GSB suspension of 5×10^5 spores/mL. **C** : Leaves of Payzawat and PI511890 stained by nitroblue tetrazolium at different time points after*S. cucurbitacearum* inoculation. **D** : Boxplots for H_2O_2 accumulation quantified by Image J at different time points after *S. cucurbitacearum* inoculation.**E** : Boxplots for O^{2-} accumulation quantified by Image J at different time points after *S. cucurbitacearum*inoculation. Least significant difference method was used for multiple comparisons of the means after ANOVA analysis. Ns represents no significance ($p > 0.05$). * represents $p < 0.05$. ** represents $p < 0.01$. *** represents $p < 0.001$.

3.3 Identification and functional enrichment analysis of DEGs

Both the growth of fungi and accumulation of H_2O_2 and O^{2-} indicated that 24 hpi is the key point to differentiate the defense responses of susceptible and resistant accessions to GSB pathogen infection. Therefore, the samples at 24 hpi were selected for full-length transcriptome sequencing. A total of 118.2 Gb clean data with an average read length of 1229.3 bp were obtained (Supplementary Table 1). The ONT reads were mapped

onto the reference genome. The expression abundance of the annotated genes was quantified using Ballgown and then DEGs were determined using DESeq2 (Figure 2A). Compared with their respective controls, 958 DEGs (457 up-regulated and 501 down-regulated) were identified for Payzawat, and 380 DEGs (344 up-regulated and 36 down-regulated) were identified for PI511890 after GSB pathogen infection. Additionally, a total of 663 DEGs were identified between Payzawat and PI511890 after GSB pathogen infection.

GO enrichment analysis showed that four terms of biological process were specifically enriched in PI511890 after infection relative to Payzawat, including hydrogen peroxide catabolic process, cell wall organization, response to wounding, and defense response (Figure 2B, Supplementary Figure2). KEGG enrichment analysis showed that three pathways (pyruvate metabolism, phenylpropanoid biosynthesis, and nitrogen metabolism) were enriched in both PI511890 and Payzawat after infection, demonstrating that these pathways are the common defense responses of melon to GSB (Figure 2C). Moreover, there were five pathways specifically enriched in PI511890 after infection, including biosynthesis of other secondary metabolites (flavonoid biosynthesis, stilbenoid, diarylheptanoid and gingerol biosynthesis, flavone and flavonol biosynthesis), MAPK signaling pathway-plant, and galactose metabolism. The DEGs enriched in the pathway of secondary metabolite synthesis were all up-regulated in GSB pathogen infected PI511890. On the other hand, 18 pathways were specifically enriched in Payzawat after infection, which included carbohydrate metabolism (glyoxylate and dicarboxylate metabolism, citrate cycle, pentose phosphate pathway, and glycolysis/gluconeogenesis), amino acid metabolism (glycine, serine and threonine metabolism, alanine, aspartate and glutamate metabolism, glutathione metabolism, arginine biosynthesis, phenylalanine metabolism, phenylalanine, tyrosine and tryptophan biosynthesis), and HIF-1 signaling pathway. These results indicated that PI511890 and Payzawat exhibit contrasting defense responses to GSB by regulating different pathways. PI511890 coped with GSB by regulating biosynthesis of secondary metabolites and MAPK signaling pathway. However, the defense response of Payzawat to GSB mainly involved carbohydrate metabolism and amino acid metabolism.

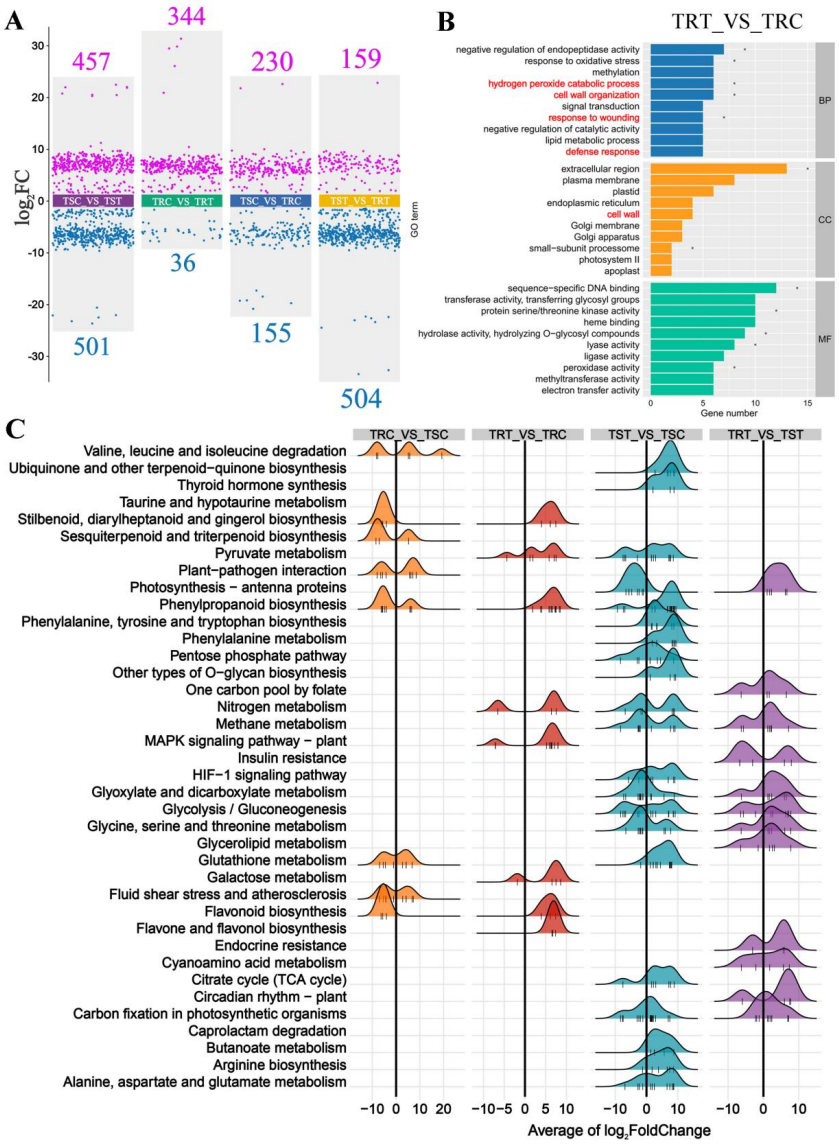

Figure 2 Identification and functional enrichment analysis of DEGs. **A** : Volcanic plots of DEGs. Red and blue points represent the up-regulated and down-regulated DEGs, respectively. **B** : GO enrichment analysis of the DEGs detected in GSB pathogen infected PI511890 compared with its control. * represents $p < 0.05$. **C:** KEGG enrichment analysis for the DEGs. TRT and TST represent GSB pathogen inoculated samples of PI511890 and Payzawat, respectively. TRC and TSC represent the controls of PI511890 and Payzawat, respectively.

3.4 Identification of isoforms and novel genes

The full-length and consensus sequences were identified and mapped onto the reference genome, resulting in over 96.37% mapping ratios (Supplementary Table 2). The mapped sequences were assembled using Stringtie, resulting in approximately 40,000 transcripts for each sample. The novel isoforms and novel genes were identified by comparing the assembled transcripts with the annotated transcripts of reference genome (Table 1). Similar numbers of isoforms of known genes were identified for the four samples. However, a larger number of novel isoforms of known genes were identified in GSB pathogen infected PI511890. More

novel genes and their isoforms were observed in GSB pathogen infected PI511890 and Payzawat compared with their controls. These results indicated that GSB infection induces the transcription of more isoforms and novel genes, particularly in the resistant genotype.

Considering their potentially important roles in regulating the defense response of melon to GSB, the novel genes were further analyzed (Figure 3A). A total of 1,071 and 1,138 novel genes were specifically identified in Payzawat and PI511890 after infection, respectively. GO enrichment analysis showed that ATP hydrolysis activity was specifically enriched in infected Payzawat, while catalytic activity was specifically enriched in infected PI511890 (Supplementary Figure 3). Moreover, KEGG enrichment analysis showed that MAPK signaling pathway was specifically enriched for the novel genes in PI511890 but not for those in Payzawat (Figure 3B). These novel genes provide new insights into the defense response of melon to GSB.

Table 1. Numbers of isoforms and novel genes identified in the full-length transcriptome.

Types	TSC	TST	TRC	TRT
Isoforms of known genes	22566	22251	22390	22509
Novel isoforms of known genes	15687	15224	15420	16375
Novel genes	1468	1535	1448	1534
Isoforms of novel genes	1946	2062	1996	2070
Total transcripts	40199	39537	39806	40954

***** TRT and TST represent GSB pathogen inoculated samples of PI511890 and Payzawat, respectively. TRC and TSC represent the controls of PI511890 and Payzawat, respectively.

3.5 Identification of AS events and fusion genes

AS serves as an important regulatory mechanism to fine-tune plant response to environmental stimuli by producing diverse transcripts. In this study, a total of 11,793 AS events including seven AS types were detected (Supplementary Figure 4). A3 and A5 were the dominant types of AS events, accounting for 43.44% and 38.86%, respectively (Figure 3C). Differential AS events were identified by calculating PSI (Supplementary Table 3). A total of 158 differential AS events were induced by GSB pathogen infection in Payzawat, which were generated by 48 annotated genes and 80 novel genes. Moreover, 117 differential AS events produced by 59 annotated genes and 46 novel genes were identified in GSB pathogen inoculated PI511890. KEGG enrichment analysis showed that the genes involved in differential AS events of Payzawat were significantly enriched in pathways related to carbohydrate metabolism, including glyoxylate and dicarboxylate metabolism, ascorbate and aldarate metabolism, and pyruvate metabolism. The pathway of RNA transport was significantly enriched for the genes involved in differential AS events in PI511890 (Supplementary Table 4). These results suggested that AS events participate in the defense responses to GSB pathogen infection in melon and exhibit significant differences between Payzawat and PI511890.

The candidate fusion genes were identified for each sample (Figure 3D). A total of 137 and 104 fusion genes were identified in the control groups of Payzawat and PI511890, respectively. After GSB pathogen infection, 129 and 118 fusion candidates were identified in Payzawat and PI511890, respectively. No significant differences were observed for the number and functional annotation of the fusion genes between the treatment and control groups. These results demonstrated that the fusion genes are probably not involved in the defense response to GSB.

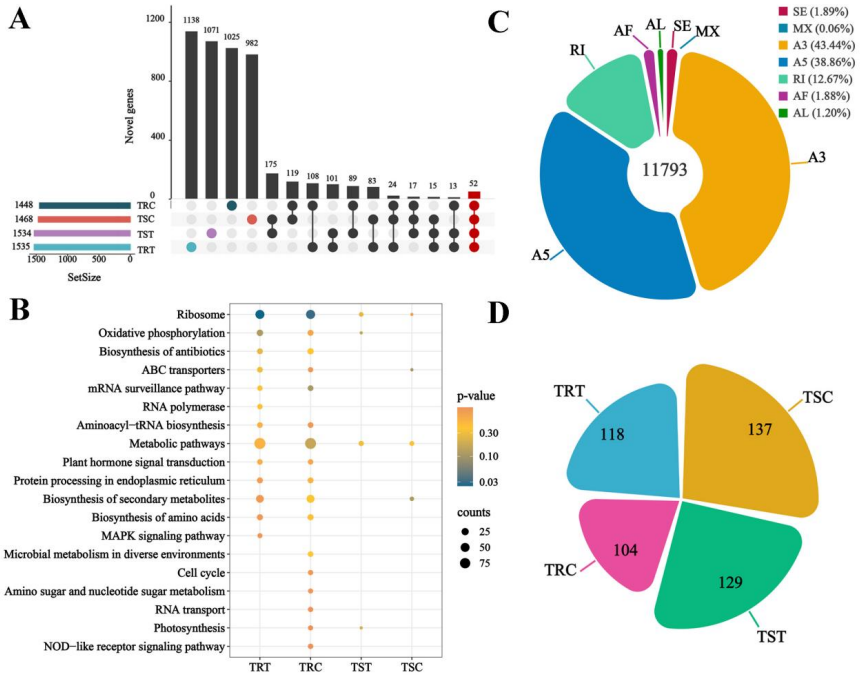

Figure 3 Results of the full-length transcriptome analysis. **A** : Number of novel genes identified in each sample. **B** : KEGG enrichment analysis of the novel genes. **C:** The predicted AS events. **D** : Number of fusion genes predicted for each sample. TRT and TST represent the samples of GSB pathogen inoculated PI511890 and Payzawat, respectively. TRC and TSC represent the controls of PI511890 and Payzawat, respectively.

3.6 Identification and functional enrichment analysis of DAMs

The samples at 24 hpi were further selected for widely targeted metabolome analysis. A total of 910 metabolites were identified, which could be divided into 11 classes (Figure 4A and Supplementary Table 5). Among them, flavonoids were the largest group, accounting for 22.53% of the total identified metabolites. Less variations were observed among biological replicates for each sample, but there were great variations between samples of Payzawat and PI511890 based on PCA analysis (Figure 4B).

A total of 132 DAMs (83 up-regulated and 49 down-regulated) were induced in PI511890 by GSB pathogen inoculation (Figure 4C), and 153 DAMs (73 up-regulated and 80 down-regulated) were detected in Payzawat. There were 36 DAMs commonly detected in PI511890 and Payzawat after GSB pathogen infection (Figure 4D). Interestingly, there were six DAMs showing completely opposite accumulation patterns in Payzawat and PI511890 (Figure 5A). Among them, oxalic acid and methyl caffeate were reported to be involved in disease resistance. The accumulation of oxalic acid was increased in resistant PI5111890 while decreased in susceptible Payzawat after GSB pathogen inoculation. An opposite accumulation pattern was observed for methyl caffeate. These results suggested that methyl caffeate is probably not directly involved in the GSB resistance. However, oxalic acid has the potential to be used as a marker metabolite for GSB resistance in melon, especially at the early stage.

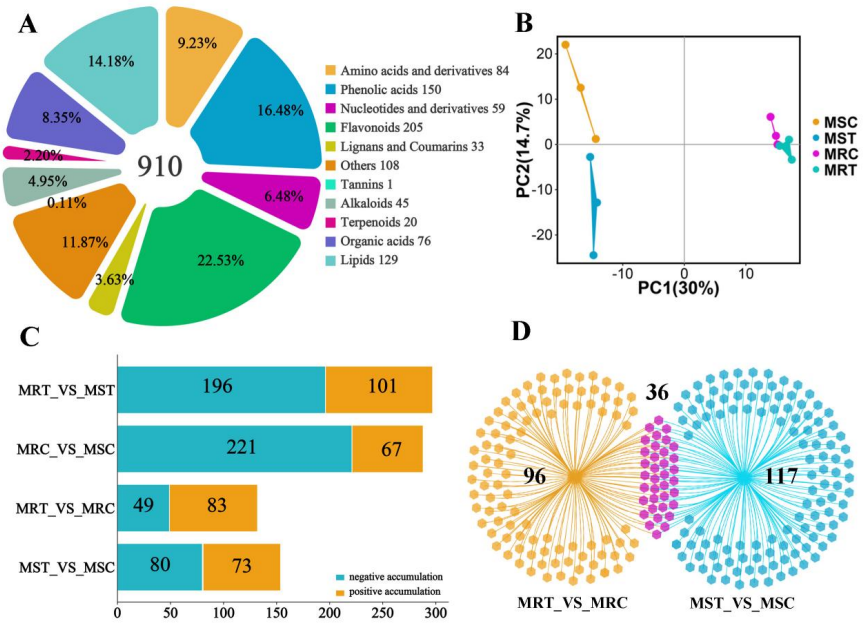

Figure 4 Classification of metabolites and identification of DAMs. **A** : Classification and composition of identified metabolites. **B** : Principal component analysis (PCA) for the samples based on the identified metabolites.**C** : Numbers of DAMs identified by pairwise comparisons.**D** : Venn diagram of DAMs identified in PI511890 and Payzawat after GSB infection. MRT and MST represent the samples of GSB pathogen inoculated PI511890 and Payzawat, respectively. MRC and MSC represent the controls of PI511890 and Payzawat, respectively.

Several flavonoids were found to be specifically accumulated in Payzawat and PI511890 after GSB infection, respectively (Figure 5B). A total of 20 flavonoids (15 up-regulated and 5 down-regulated) were specifically induced in Payzawat, among which apigenin and its derivatives were the most abundant. Moreover, there were 23 flavonoids (17 up-regulated and 6 down-regulated) specifically induced in PI511890. Among them, chrysoeriol and its derivatives were the most abundant. These results suggested that GSB pathogen infection induces significant changes in the species and content of flavonoids in Payzawat and PI511890. Moreover, chrysoeriol and its derivatives also have the potential to be used as marker metabolites for GSB resistance in melon.

KEGG enrichment analysis of DAMs showed that seven pathways were enriched in both PI511890 and Payzawat after infection, including amino acid metabolism (alanine, aspartate and glutamate metabolism, phenylalanine metabolism), carbohydrate metabolism (C5-Branched dibasic acid metabolism, glyoxylate and dicarboxylate metabolism), biosynthesis of other secondary metabolites (flavonoid biosynthesis), chemical structure transformation maps (biosynthesis of plant hormones, and biosynthesis of phenylpropanoids) (Figure 5C). The results indicated that these pathways are involved in the common defense response of melon to GSB. Moreover, there were nine pathways specifically enriched in PI511890 after infection, including amino acid metabolism (tryptophan metabolism, phenylalanine, tyrosine and tryptophan biosynthesis), membrane transport (phosphotransferase system, ABC transporters), carbohydrate metabolism (ascorbate and aldarate metabolism), biosynthesis of secondary metabolites, metabolism of cofactors and vitamins. On the other hand, 11 pathways were specifically enriched in Payzawat after infection, such as biosynthesis of other secondary metabolites (flavone and flavonol biosynthesis), carbohydrate metabolism (pentose phosphate pathway, butanoate metabolism), lipid metabolism (linoleic acid metabolism), amino acid metabolism (lysine biosynthesis, glutathione metabolism), metabolism of cofactors and vitamins (vitamin B6 metabolism),

and PPAR signaling pathway. These results demonstrated that PI511890 and Payzawat exhibit contrasting defense responses to GSB by regulating different metabolic pathways.

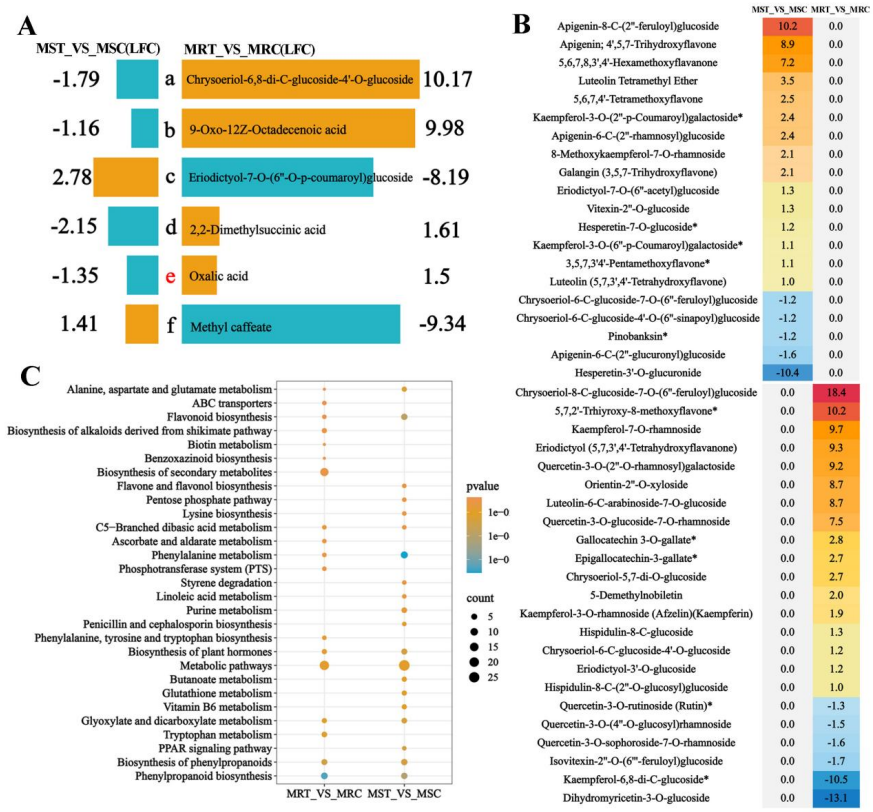

Figure 5 KEGG enrichment analysis of DAMs and in-depth analysis of key metabolites. **A** : Six DAMs (a-f) with opposite accumulation patterns in Payzawat and PI511890. The horizontal axis indicates the value of $\log_2$FoldChange. Blue bars represent the down-regulated DAMs. Orange bars represent up-regulated DAMs. **B** : Flavonoids specifically accumulated in Payzawat and PI511890 after GSB pathogen infection. **C** : KEGG enrichment analysis for DAMs. MRT and MST represent the samples of GSB pathogen inoculated PI511890 and Payzawat, respectively. MRC and MSC represent the controls of PI511890 and Payzawat, respectively.

3.7 Integration of transcriptome and metabolome profiles

To systematically understand the defense response of melon to GSB at both transcriptomic and metabolic levels, an integrated transcriptome and metabolome analysis was performed. A total of eight and 18 KEGG pathways were significantly enriched in transcriptome and metabolome in PI511890 after infection, respectively (Figure 6A). However, only phenylpropanoid biosynthesis and flavonoid biosynthesis were commonly enriched for both DEGs and DAMs in PI511890 after infection. Similarly, a total of 21 and 20 KEGG pathways were enriched for DEGs and DAMs in Payzawat after infection, respectively (Figure 6A). Several pathways, including amino acid metabolism (alanine, aspartate and glutamate metabolism, phenylalanine metabolism, butanoate metabolism, glutathione metabolism), carbohydrate metabolism (pentose phosphate pathway, glyoxylate and dicarboxylate metabolism), and biosynthesis of other secondary metabolites (phenylpropanoid biosynthesis, phenylalanine, tyrosine and tryptophan biosynthesis, flavone and flavonol biosynthesis), were commonly enriched in transcriptome and metabolome in Payzawat after infection.

Since phenylpropanoid biosynthesis was the only pathway commonly enriched for DEGs and DAMs in both PI511890 and Payzawat after GSB pathogen infection, the profiles of genes and metabolites in this pathway

were further analyzed (Figure 6). Except for the gene encoding chalcone isomerase (*MELO3C016680.2*) that was down regulated in PI511890, the other genes were mainly upregulated in both PI511890 and Payzawat after GSB pathogen infection. Accumulation of lignins decreased in PI511890 but not changed in Payzawat. Accumulation of eriodictyol specifically increased in PI511890, while apigenin specifically increased in Payzawat. Furthermore, glyoxylate and dicarboxylate metabolism and metabolic pathways were also enriched in transcriptome and metabolome, in which the accumulation of oxalic acid in PI511890 was significantly upregulated in glyoxylate cycle and citric acid cycle (TCA cycle) (Supplementary Figure 5, Supplementary Figure 6). These results demonstrated that eriodictyol and oxalic acid have the potential to be used as marker metabolites for GSB resistance in melon. Moreover, the inconsistency of gene expression patterns and the related metabolite accumulation patterns suggested that post-transcription regulation is widely involved in the defense response of melon to GSB.

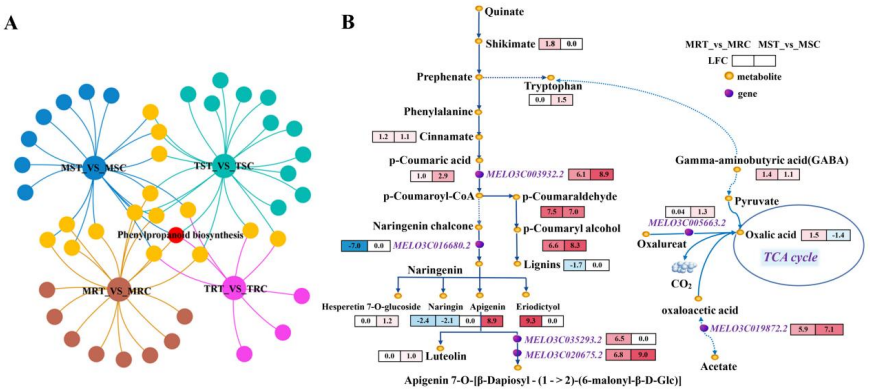

Figure 6 Integrated analysis of transcriptome and metabolome. **A:** Venn diagram of KEGG pathways enriched for DEGs and DAMs in Payzawat and PI511890. **B:** Diagram of partial regulatory pathways for genes and metabolites. Yellow nodes are metabolites, and purple nodes are genes. The values of LFC for key DEGs and DAMs are marked. MRT and MST represent the samples of GSB pathogen inoculated PI511890 and Payzawat, respectively. MRC and MSC represent the controls of PI511890 and Payzawat, respectively.

4. Discussion

GSB is a prevalent fungal disease not only for melon but also for most commonly cultivated cucurbits, which is also considered as a potential risk in the global movement of plant pathogens as it can be on or in seeds and transplants (Seblani et al., 2023). Several GSB resistant resources and related inheritance of resistant genes have been identified in melon (Luo et al., 2022). However, the interaction between melon and GSB and the related disease resistance mechanism are still unknown, which impedes genetic improvement of melon with GSB resistance. To address these problems, full-length transcriptome, metabolome, and histochemical staining methods were used in this study to reveal the early defense response of melon to GSB.

Plants cope with pathogen attack through the innate immune response initiated by cell surface-localized pattern-recognition receptors (PRRs) and intracellular nucleotide-binding domain leucine-rich repeat containing receptors (NLRs), which trigger pattern-triggered immunity (PTI) and effector-triggered immunity (ETI), respectively (Yuan et al., 2021). Upon recognition of pathogen or microbe-associated molecular patterns (PAMPs/MAMPs), cell surface-localized PRRs recruit co-receptors to form receptor complexes and activate downstream phosphorylate receptor-like cytoplasmic kinases (Liang & Zhou, 2018), which subsequently phosphorylate downstream components to trigger ROS burst, Ca^{2+} influx, MAPK activation, phytohormone production, and transcriptional reprograming. NLRs form resistosomes upon activation, which eventually leads to multiple immune responses (Yuan et al., 2021). Several studies have also shown that plant MAPK cascades play pivotal roles in signaling plant defense against pathogen attack (Zhang & Zhang, 2022). In this study, through staining experiments, we found that the growth of *S. cucurbitacearum* was

significantly inhibited in PI511890, and O^{2-} and H_2O_2 were accumulated significantly at 24 hpi. DEGs including novel genes were specifically enriched in the MAPK signaling pathway in PI511890, indicating that the MAPK signaling pathway is involved in the resistance of melon to GSB pathogen infection. Additionally, GO enrichment analysis showed that hydrogen peroxide catabolic process, cell wall organization, response to wounding, and defense response were significantly enriched in PI511890, suggesting that PI511890 inhibits *S. cucurbitacearum* invasion probably by catabolizing hydrogen peroxide and preventing pathogenic fungi to destroy cell wall.

The inherent advantage of full-length transcriptome makes it possible to understand the complexity of AS events at the whole genome scale. AS is an important modulator of gene expression that can increase proteome diversity (Ule & Blencowe, 2019). In this study, 11793 AS events including seven types were detected, which followed an order of A3 > A5 > RI > SE > AF > AL > MX in the number of members. Moreover, 158 differential AS events were related to carbohydrate metabolism in Payzawat after GSB pathogen infection, while 117 differential AS events were related to RNA transport in PI511890 after infection. These results demonstrated that AS events are widely involved in the early response of melon to GSB infection.

It has been reported that oxalic acid has a protective effect against pathogen attack (Palmieri et al., 2019; Schmalenberger et al., 2015). In this study, oxalic acid was positively accumulated in PI511890, while decreased in Payzawat after GSB pathogen infection. In the pathway of glyoxylate and dicarboxylate metabolism enriched by DEGs, the positively accumulated oxalic acid was derived from the glyoxylate cycle. Moreover, the pathway of chloroalkane and chloroalkane degradation, which promotes the accumulation of oxalic acid, was also enriched by DAMs in PI511890 after GSB pathogen infection. The pathways enriched by both DEGs and DAMs, as well as the significantly increased accumulation of oxalic acid induced by GSB in PI511890, demonstrated that oxalic acid can be used as a metabolite mark for GSB resistance in melon.

Lignin acts as a passive physical barrier (Lee et al., 2019; Vanholme et al., 2019), and reduction of its synthesis can relax cell wall structure to facilitate the release of DAMPs by pathogens (Savatin et al., 2014; Xiao et al., 2021), thereby initiating the immune response of plants to enhance disease resistance. In this study, lignin content in PI511890 was lower than that in Payzawat after GBS pathogen infection, suggesting that lignin is also involved in the GSB resistance in melon. Additionally, flavonoid metabolites have multifaceted roles in mediating plant-microbe interactions (Wang et al., 2022). The differentially accumulated flavonoids differed between PI511890 and Payzawat after GSB pathogen infection. Eriodictyol was specifically accumulated in infected PI511890 and apigenin was specifically accumulated in infected Payzawat. It is currently unknown how these two metabolites contribute to the GSB resistance, but the discrepancy between them must be related to the difference in GSB resistance between PI511890 and Payzawat.

Combined transcriptome and metabolome analysis provides an important approach for the mining of metabolic networks and key genes (Gong et al., 2021; Wei et al., 2016). In this study, we established the relationship between DEGs and DAMs, and found that eriodictyol and oxalic acid have the potential to be used as marker metabolites for GSB resistance in melon. However, no significant correlations were observed between accumulation patterns of DAMs and expression profiles of DEGs in the same enriched pathways. These results demonstrated that post-transcription regulation is widely involved in the defense response of melon to GSB. This study provides some insights and theoretical basis for understanding the resistance mechanism of melon to GSB. However, the specific disease resistance mechanism and relevant effectors remain to be further explored. Thus, other multi-omics studies should be incorporated to establish a more comprehensive metabolic regulatory network for understanding the resistance of melon to GSB.

Funding

This work was supported by the Key R&D project of Hubei Province (2021BBA101), the Fundamental Research Funds for the Central Universities (2662020YLPY024), the Major Project of Sci & Tech of Xinjiang (2022A03004-5), and the China Agriculture Research System (CARS-25-G2).

Author contributions

Q.K. conceived and designed the study and revised the manuscript. Y.Z. and X.Z. provided the plant materials. H.W. participated in data analysis, writing and revising the manuscript. X.W. participated in sampling and sequencing. C.M. and M.W. participated in data analysis. Y.L., Y.F., and X.G. contributed to the preparation of plant samples. All authors read and approved the final manuscript.

Data availability

Sequencing data of full-length transcriptome form the Oxford Nanopore Technologies (ONT) have been submitted to BioProject of PRJNA1039169 in the National Center for Biotechnology Information (NCBI). The other datasets generated and/or analyzed during the current study are available from the corresponding author on reasonable request.

Competing interests

The authors declare that they have no conflict of interest.

References

Anjali, S., Kumar, S., Korra, T., Thakur, R., Arutselvan, R., Kashyap, A. S., et al. (2023). Role of plant secondary metabolites in defence and transcriptional regulation in response to biotic stress. *Plant Stress, 8* , 100154-Article No.: 100154. doi:10.1016/j.stress.2023.100154

Bhadauria, V., Miraz, P., Kennedy, R., Banniza, S., & Wei, Y. (2010). Dual trypan-aniline blue fluorescence staining methods for studying fungus-plant interactions. *Biotech Histochem, 85* (2), 99-105. doi:10.1080/10520290903132196

Chen, C., Zhou, G., Chen, J., Liu, X., Lu, X., Chen, H., & Tian, Y. (2021). Integrated Metabolome and Transcriptome Analysis Unveils Novel Pathway Involved in the Formation of Yellow Peel in Cucumber. *Int J Mol Sci, 22* (3). doi:10.3390/ijms22031494

Chen, W., Gong, L., Guo, Z., Wang, W., Zhang, H., Liu, X., et al. (2013). A novel integrated method for large-scale detection, identification, and quantification of widely targeted metabolites: application in the study of rice metabolomics. *Mol Plant, 6* (6), 1769-1780. doi:10.1093/mp/sst080

Daudi, A., & O'Brien, J. A. (2012). Detection of Hydrogen Peroxide by DAB Staining in Arabidopsis Leaves. *Bio Protoc, 2* (18).

De Coster, W., D'Hert, S., Schultz, D. T., Cruts, M., & Van Broeckhoven, C. (2018). NanoPack: visualizing and processing long-read sequencing data. *Bioinformatics, 34* (15), 2666-2669. doi:10.1093/bioinformatics/bty149

Eriksson, L., Andersson, P. L., Johansson, E., & Tysklind, M. (2006). Megavariate analysis of environmental QSAR data. Part I–a basic framework founded on principal component analysis (PCA), partial least squares (PLS), and statistical molecular design (SMD). *Mol Divers, 10* (2), 169-186. doi:10.1007/s11030-006-9024-6

Frantz, J. D., & Jahn, M. M. (2004). Five independent loci each control monogenic resistance to gummy stem blight in melon (*Cucumis melo*L.). *Theor Appl Genet, 108* (6), 1033-1038. doi:10.1007/s00122-003-1519-2

Gong, C., Diao, W., Zhu, H., Umer, M. J., Zhao, S., He, N., et al. (2021). Metabolome and Transcriptome Integration Reveals Insights Into Flavor Formation of 'Crimson' Watermelon Flesh During Fruit Development. Frontiers in Plant Science, 12. doi:10.3389/fpls.2021.629361

Hassan, M. Z., Rahim, M. A., Natarajan, S., Robin, A. H. K., Kim, H.-T., Park, J.-I., & Nou, I.-S. (2018). Gummy Stem Blight Resistance in Melon: Inheritance Pattern and Development of Molecular Markers.*International Journal of Molecular Sciences, 19* (10). doi:10.3390/ijms19102914

Hassan, M. Z., Robin, A. H. K., Rahim, M. A., Natarajan, S., Kim, H.-T., Park, J.-I., & Nou, I.-S. (2018). Screening of melon genotypes identifies gummy stem blight resistance associated with Gsb1 resistant loci. *Journal of Plant Biotechnology, 45* (3), 217-227. doi:10.5010/jpb.2018.45.3.217

Hu, Y., Huang, Y., Du, Y., Orellana, C. F., Singh, D., Johnson, A. R., et al. (2013). DiffSplice: the genome-wide detection of differential splicing events with RNA-seq. *Nucleic Acids Res, 41* (2), e39. doi:10.1093/nar/gks1026

Hu, Z., Deng, G., Mou, H., Xu, Y., Chen, L., Yang, J., & Zhang, M. (2018). A re-sequencing-based ultra-dense genetic map reveals a gummy stem blight resistance-associated gene in *Cucumis melo* . *DNA Research, 25* (1), 1-10. doi:10.1093/dnares/dsx033

Keinath, A. P., & Zitter, T. A. (1998). Resistance to Benomyl and Thiophanate-methyl in *Didymella bryoniae* from South Carolina and New York. *Plant Dis, 82* (5), 479-484. doi:10.1094/pdis.1998.82.5.479

Kufel, J., Diachenko, N., & Golisz, A. (2022). Alternative splicing as a key player in the fine-tuning of the immunity response in Arabidopsis.*Molecular Plant Pathology, 23* (8), 1226-1238. doi:10.1111/mpp.13228

Lee, M. H., Jeon, H. S., Kim, S. H., Chung, J. H., Roppolo, D., Lee, H. J., et al. (2019). Lignin-based barrier restricts pathogens to the infection site and confers resistance in plants. *Embo j, 38* (23), e101948. doi:10.15252/embj.2019101948

Li, H.-X., Gottilla, T. M., & Brewer, M. T. (2017). Organization and evolution of mating-type genes in three Stagonosporopsis species causing gummy stem blight of cucurbits and leaf spot and dry rot of papaya.*Fungal Biology, 121* (10), 849-857. doi:10.1016/j.funbio.2017.06.002

Li, H. (2018). Minimap2: pairwise alignment for nucleotide sequences.*Bioinformatics, 34* (18), 3094-3100. doi:10.1093/bioinformatics/bty191

Li, H., Fan, C., Liu, J., Wang, B., & Li, H. (2022). Integration of full-length transcriptomes and anthocyanin metabolite analysis for understanding fruit coloration mechanism in *Schisandra chinensis* .*Physiol Mol Biol Plants, 28* (5), 921-933. doi:10.1007/s12298-022-01179-3

Liang, X., & Zhou, J. M. (2018). Receptor-Like Cytoplasmic Kinases: Central Players in Plant Receptor Kinase-Mediated Signaling. *Annu Rev Plant Biol, 69* , 267-299. doi:10.1146/annurev-arplant-042817-040540

Liu, S., Wang, Z., Zhu, R., Wang, F., Cheng, Y., & Liu, Y. (2021). Three Differential Expression Analysis Methods for RNA Sequencing: limma, EdgeR, DESeq2. *J Vis Exp* (175). doi:10.3791/62528

López-Ibáñez, J., Pazos, F., & Chagoyen, M. (2016). MBROLE 2.0-functional enrichment of chemical compounds. *Nucleic Acids Res, 44* (W1), W201-204. doi:10.1093/nar/gkw253

Luo, Q., Tan, G.-F., Ma, Y.-Q., Meng, P.-H., & Zhang, J. (2022). Cucurbitaceous Vegetables' Gummy Stem Blight Research.*Agronomy-Basel, 12* (6). doi:10.3390/agronomy12061283

Ma, J., Li, C., Tian, J., Qiu, Y., Geng, L., & Wang, J. (2023). Identification and Fine Mapping of Gummy Stem Blight Resistance Gene*Gsb-7(t)* in Melon. *Phytopathology, 113* (5), 858-865. doi:10.1094/phyto-05-22-0169-r

Mei, C., Yang, J., Yan, P., Li, N., Ma, K., Mamat, A., et al. (2020). Full-length transcriptome and targeted metabolome analyses provide insights into defense mechanisms of Malus sieversii against*Agrilus mali* . *PeerJ, 8* , e8992. doi:10.7717/peerj.8992

Palmieri, F., Estoppey, A., House, G. L., Lohberger, A., Bindschedler, S., Chain, P. S. G., & Junier, P. (2019). Oxalic acid, a molecule at the crossroads of bacterial-fungal interactions. *Adv Appl Microbiol, 106* , 49-77. doi:10.1016/bs.aambs.2018.10.001

Patro, R., Duggal, G., Love, M. I., Irizarry, R. A., & Kingsford, C. (2017). Salmon provides fast and bias-aware quantification of transcript expression. *Nat Methods, 14* (4), 417-419. doi:10.1038/nmeth.4197

Pertea, G., & Pertea, M. (2020). GFF Utilities: GffRead and GffCompare.*F1000Res, 9* . doi:10.12688/f1000research.23297.2

Pertea, M., Kim, D., Pertea, G. M., Leek, J. T., & Salzberg, S. L. (2016). Transcript-level expression analysis of RNA-seq experiments with HISAT, StringTie and Ballgown. *Nat Protoc, 11* (9), 1650-1667. doi:10.1038/nprot.2016.095

Pertea, M., Pertea, G. M., Antonescu, C. M., Chang, T. C., Mendell, J. T., & Salzberg, S. L. (2015). StringTie enables improved reconstruction of a transcriptome from RNA-seq reads. *Nat Biotechnol, 33* (3), 290-295. doi:10.1038/nbt.3122

Rennberger, G., & Keinath, A. P. (2018). Susceptibility of Fourteen New Cucurbit Species to Gummy Stem Blight Caused by *Stagonosporopsis citrulli* Under Field Conditions. *Plant Disease, 102* (7), 1365-1375. doi:10.1094/pdis-12-17-1953-re

Savatin, D. V., Gramegna, G., Modesti, V., & Cervone, F. (2014). Wounding in the plant tissue: the defense of a dangerous passage.*Front Plant Sci, 5* , 470. doi:10.3389/fpls.2014.00470

Schmalenberger, A., Duran, A. L., Bray, A. W., Bridge, J., Bonneville, S., Benning, L. G., et al. (2015). Oxalate secretion by ectomycorrhizal Paxillus involutus is mineral-specific and controls calcium weathering from minerals. *Sci Rep, 5* , 12187. doi:10.1038/srep12187

Schneider, C. A., Rasband, W. S., & Eliceiri, K. W. (2012). NIH Image to ImageJ: 25 years of image analysis. *Nat Methods, 9* (7), 671-675. doi:10.1038/nmeth.2089

Seblani, R., Keinath, A. P., & Munkvold, G. (2023). Gummy stem blight: One disease, three pathogens. *Molecular Plant Pathology* . doi:10.1111/mpp.13339

Serag, A., Salem, M. A., Gong, S., Wu, J.-L., & Farag, M. A. (2023). Decoding Metabolic Reprogramming in Plants under Pathogen Attacks, a Comprehensive Review of Emerging Metabolomics Technologies to Maximize Their Applications. *Metabolites, 13* (3). doi:10.3390/metabo13030424

Stewart, J. E., Turner, A. N., & Brewer, M. T. (2015). Evolutionary history and variation in host range of three Stagonosporopsis species causing gummy stem blight of cucurbits. *Fungal Biology, 119* (5), 370-382. doi:10.1016/j.funbio.2014.12.008

Trincado, J. L., Entizne, J. C., Hysenaj, G., Singh, B., Skalic, M., Elliott, D. J., & Eyras, E. (2018). SUPPA2: fast, accurate, and uncertainty-aware differential splicing analysis across multiple conditions. *Genome Biol, 19* (1), 40. doi:10.1186/s13059-018-1417-1

Ule, J., & Blencowe, B. J. (2019). Alternative Splicing Regulatory Networks: Functions, Mechanisms, and Evolution. *Mol Cell, 76* (2), 329-345. doi:10.1016/j.molcel.2019.09.017

van Wees, S. (2008). Phenotypic analysis of Arabidopsis mutants: trypan blue stain for fungi, oomycetes, and dead plant cells. *CSH Protoc, 2008* , pdb.prot4982. doi:10.1101/pdb.prot4982

Vanholme, R., De Meester, B., Ralph, J., & Boerjan, W. (2019). Lignin biosynthesis and its integration into metabolism. *Curr Opin Biotechnol, 56* , 230-239. doi:10.1016/j.copbio.2019.02.018

Virtuoso, M. C. S., Valente, T. S., Costa Silva, E. H., Braz, L. T., Panizzi, R. d. C., & Vargas, P. F. (2022). Implications of the inoculation method and environment in the selection of melon genotypes resistant to Didymella bryoniae. *Scientia Horticulturae, 300* . doi:10.1016/j.scienta.2022.111066

Wang, L., Chen, M., Lam, P. Y., Dini-Andreote, F., Dai, L., & Wei, Z. (2022). Multifaceted roles of flavonoids mediating plant-microbe interactions. Microbiome, 10(1), 233. doi:10.1186/s40168-022-01420-x

Wei, G., Tian, P., Zhang, F., Qin, H., Miao, H., Chen, Q., et al. (2016). Integrative Analyses of Nontargeted Volatile Profiling and Transcriptome Data Provide Molecular Insight into VOC Diversity in Cucumber Plants (*Cucumis sativus*). Plant Physiology, 172(1), 603-618. doi:10.1104/pp.16.01051

Wolukau, J. N., Zhou, X.-H., Li, Y., Zhang, Y.-B., & Chen, J.-F. (2007). Resistance to gummy stem blight in melon (*Cucumis melo*L.) germplasm and inheritance of resistance from plant introductions 157076, 420145,

and 323498. *Hortscience, 42* (2), 215-221. doi:10.21273/hortsci.42.2.215

Wolukau, J. N., Zhou, X., & Chen, J. (2009). Identification of Amplified Fragment Length Polymorphism Markers Linked to Gummy Stem Blight (*Didymella bryoniae*) Resistance in Melon (Cucumis melo L.) PI 420145. *Hortscience, 44* (1), 32-34. doi:10.21273/hortsci.44.1.32

Xiao, S., Hu, Q., Shen, J., Liu, S., Yang, Z., Chen, K., et al. (2021). GhMYB4 downregulates lignin biosynthesis and enhances cotton resistance to *Verticillium dahliae* . *Plant Cell Rep, 40* (4), 735-751. doi:10.1007/s00299-021-02672-x

Yu, G., Wang, L. G., Han, Y., & He, Q. Y. (2012). clusterProfiler: an R package for comparing biological themes among gene clusters.*Omics, 16* (5), 284-287. doi:10.1089/omi.2011.0118

Yuan, M., Ngou, B. P. M., Ding, P., & Xin, X. F. (2021). PTI-ETI crosstalk: an integrative view of plant immunity. *Curr Opin Plant Biol, 62* , 102030. doi:10.1016/j.pbi.2021.102030

Zhang, H., Mao, R., Wang, Y., Zhang, L., Wang, C., Lv, S., et al. (2019). Transcriptome-wide alternative splicing modulation during plant-pathogen interactions in wheat. *Plant Science, 288* . doi:10.1016/j.plantsci.2019.05.023

Zhang, Y. P., Kyle, M., Anagnostou, K., & Zitter, T. A. (1997). Screening melon (*Cucumis melo*) for resistance to gummy stem blight in the greenhouse and field. *Hortscience, 32* (1), 117-121. doi:10.21273/hortsci.32.1.117

Zhao, Q., Gong, Z., Jiang, S., Li, Z., Zhang, L., Wang, L., et al. (2022). Gene mining to discover pumpkin response genes to gummy stem blight infection caused by *Stagonosporopsis cucurbitacearum* .*Journal of Plant Interactions, 17* (1), 1-8. doi:10.1080/17429145.2021.2006331

Zhang, M., & Zhang, S. (2022). Mitogen-activated protein kinase cascades in plant signaling. J Integr Plant Biol, 64(2), 301-341. doi:10.1111/jipb.13215

Tables

Table 1. Numbers of isoforms and novel genes identified in the full-length transcriptome.

Figures

Figure 1. Growth of GSB pathogenic fungi and accumulation of H_2O_2 and O^{2-} in leaves of PI511890 and Payzawat.

Figure 2. Identification and functional enrichment analysis of DEGs.

Figure 3. Results of the full-length transcriptome analysis.

Figure 4. Classification of metabolites and identification of DAMs.

Figure 5. KEGG enrichment analysis of DAMs and in-depth analysis of key metabolites.

Figure 6. Integrated analysis of transcriptome and metabolome.

Supplemental materials

Supplementary Table 1. Statistics of the full-length transcriptome sequencing data.

Supplementary Table 2. Results statistics of the alignment to the DHL92_v4.0 reference genome.

Supplementary Table 3. Differential AS events after pathogen infection in susceptible and resistant materials.

Supplementary Table 4. The KEGG pathway enrichment of differential AS events.

Supplementary Table 5. Classification and content of the 910 metabolites.

Supplementary Figure 1. Flow of the full-length transcriptome analysis.

Supplementary Figure 2. The GO enrichment analysis of DEGs in Payzawat after infection.

Supplementary Figure 3. The GO enrichment analysis of novel genes in four groups.

Supplementary Figure 4. Seven types and proportion of alternative splicing events.

Supplementary Figure 5. Pathway diagram of metabolic pathways (map00625).

Supplementary Figure 6. Pathway diagram of chloroalkane and chloroalkane degradation (map01100).

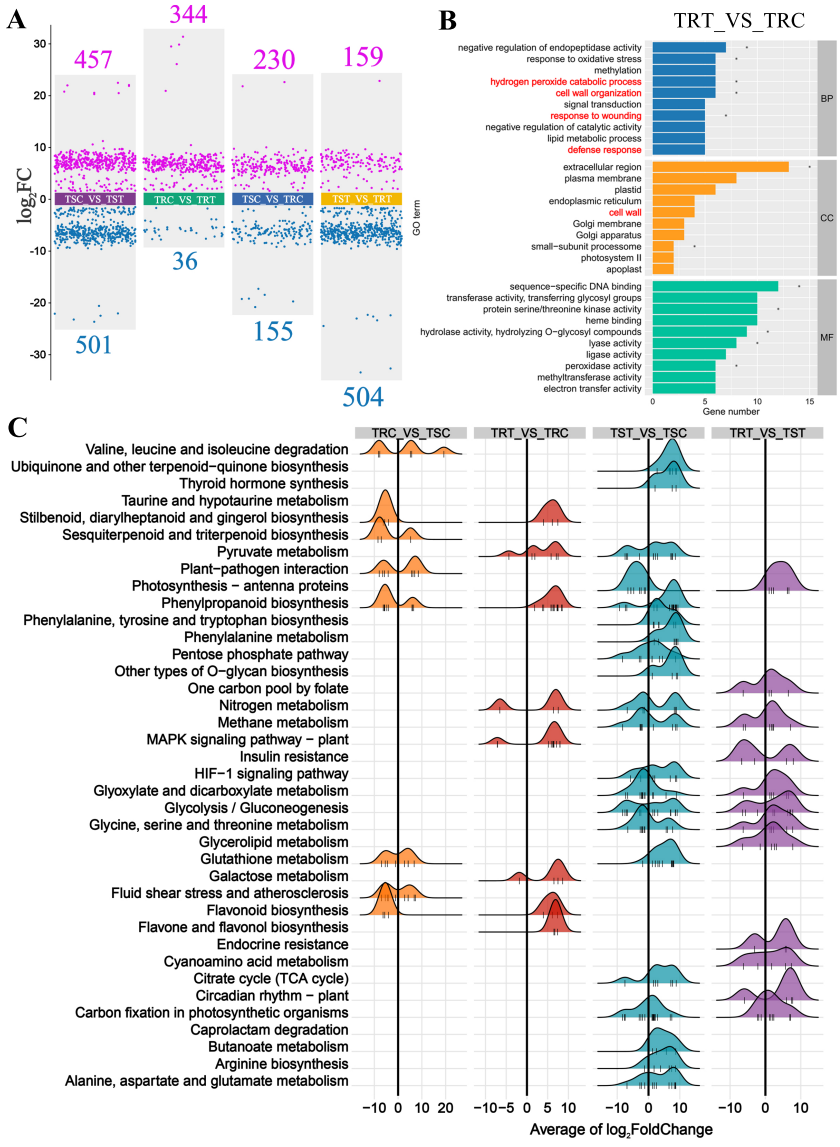

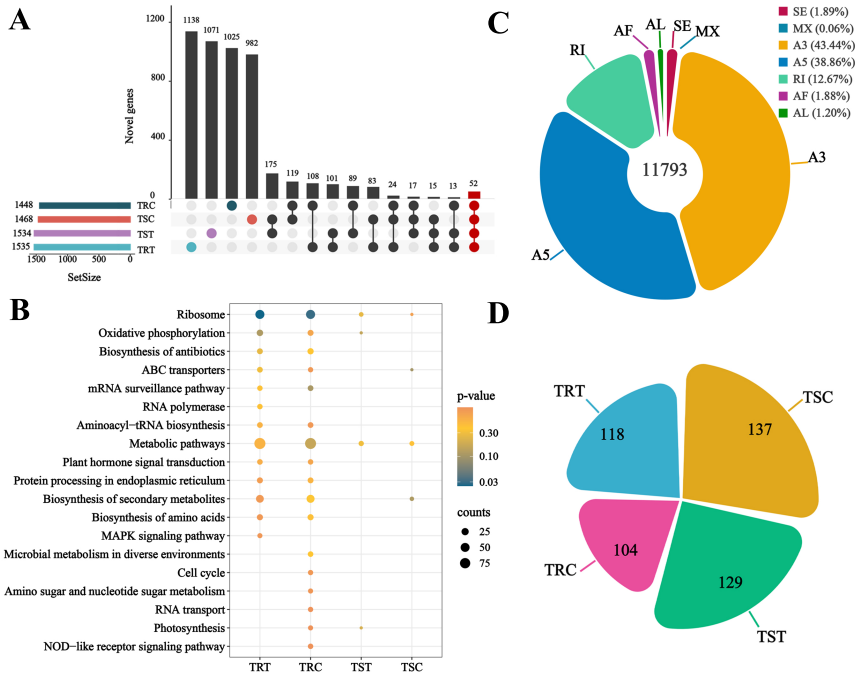

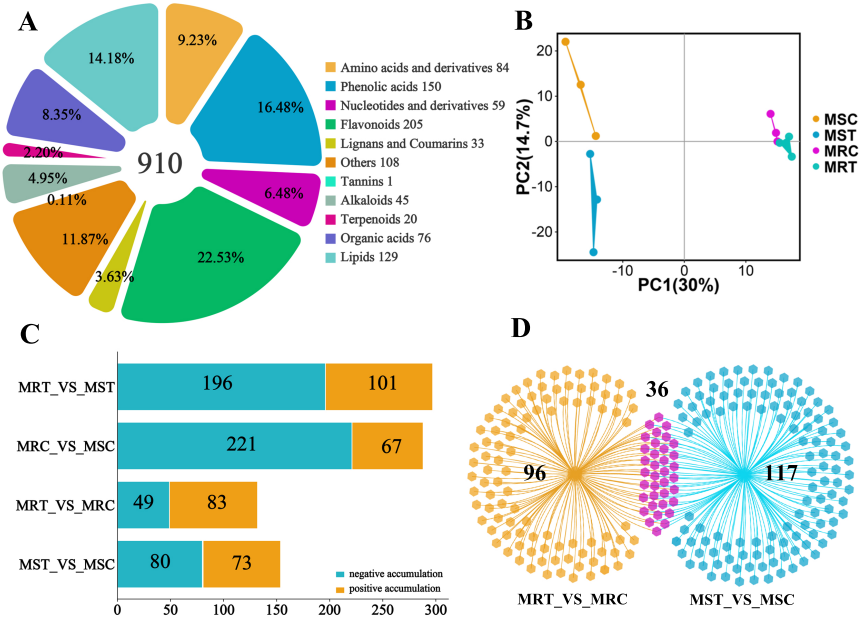

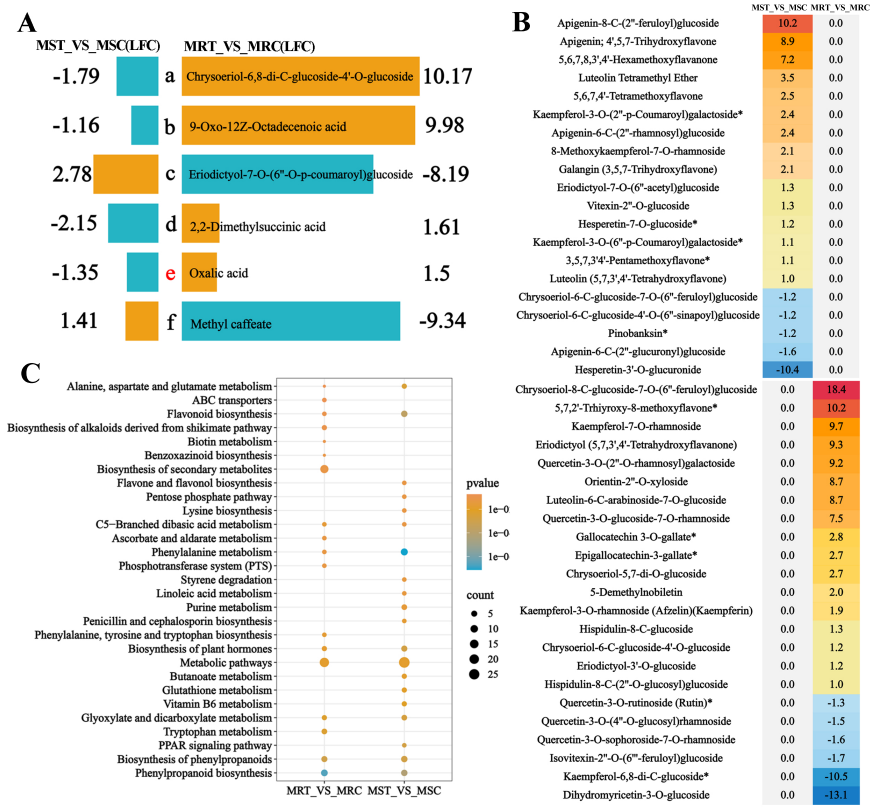

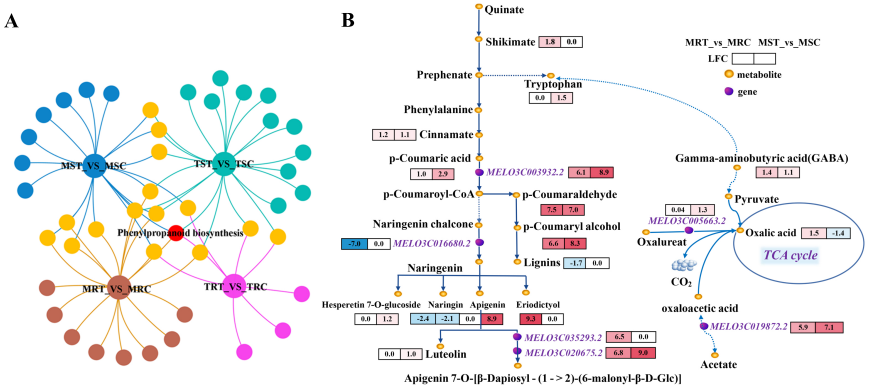

A

0 h 12 h 24 h 36 h 48 h 60 h 72 h

Payzawat

PI511890

B

12h 24h 36h 48h

Payzawat

Control

Treatment

PI511890

Control

Treatment

C

12h 24h 36h 48h

Payzawat

Control

Treatment

PI511890

Control

Treatment

D

12 h 24 h

36 h 48 h

The accumulated area of H_2O_2 (%)

ns * ** ***

E

12 h 24 h

36 h 48 h

The accumulated area of O^{2-} (%)

ns * ** ***

Paytawat-Control

Paytawat-Treatment

PI511890-Control

PI511890-Treatment